SUPERCONDUCTIVITY – *Applied*

Influence of Void Fraction on AC Loss in NbTi Cable-In-Conduit Conductor

Baudouy, B., NHMFL
Takeda, M., Kobe Univ. of Mercantile Marine, Japan
Van Sciver, S., NHMFL/FAMU-FSU College of
  Engineering

AC loss measurements have been carried out on NbTi Cable-In-Conduit conductor[1] (CICC) to investigate the effect of void fraction. Tests were conducted using the Test of AC Loss (TACL) facility that consists of a 7 T superconducting dipole magnet with an insulated insert cryostat operating around 1.8 K. The magnetic field produced is perpendicular to the conductor axis and no transport current is applied to the sample. The AC pulse is achieved by a rapid discharge of the current through a dump resistor. Tests were performed for three different initial fields (1 T, 3 T and 5T) and for four different field sweep rates. AC loss is determined by measuring the temperature or enthalpy change of the He II surrounding the conductor.[2] The analysis of the data is based on the assumption that, in our measurement frequency range, the losses are dominated by magnetic hysteresis and by induced coupling current within and among the cable strands. The total energy dissipation is the sum of these two contributions. Figure 1 shows the total losses in the conductor for 40% and 50% void fractions as a function of the applied field sweep rate, dB/dt, at different initial magnetic fields. AC loss are higher for a void fraction of 40%. Analysis of the total losses shows that the hysteresis term is constantly independent of the void fraction since it results from filament magnetization. The analysis shows also that the coupling current term is higher for the 40% void fraction conductor since the lower void fraction improves contact between strands. Figure 1 shows also that these conductors exhibit a "saturation effect."[3] At high field sweep rates, the filament can locally carry the current density, and the power generated by the coupling current loss
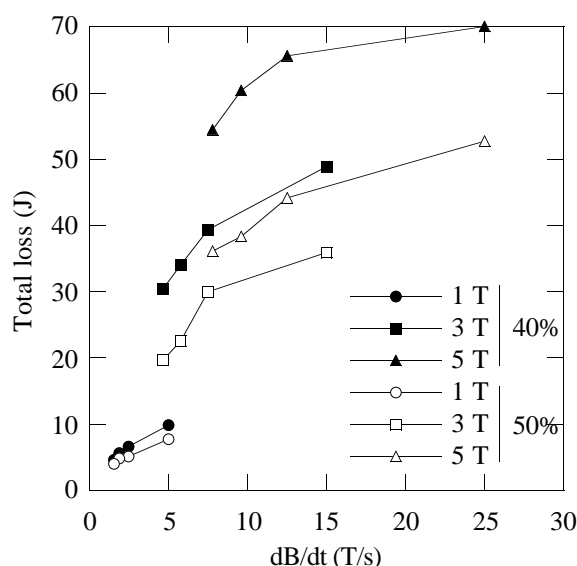

Figure 1. Total loss as a function of field sweep rate for different void fractions.

is no longer proportional to the square of the filed sweep rate (dB/dt).[2]

References:

[1]   Baudouy, B., *et al.*, Ad. Cryo. Eng., **41A**, 397 (1996).
[2]   Baudouy, B., *et al.*, IEEE Trans. on App. Supercond., **5**, 2, 688 (June 1995).
[3]   Bonito Oliva, A., *et al.*, IEEE Trans. on Magn., **32**, 4, 2834 (1996).

Three-Dimensional Numerical Analyses of the Stability of Ag/BSCCO Tape Conductors

Burkhardt, E.E., NHMFL/Univ. of Illinois
Schwartz, J., NHMFL/FAMU-FSU College of
   Engineering

The stability of superconducting magnets subjected to external thermal disturbances or flux jumps depends on the interplay between the electromagnetic and thermal characteristics of the system. Here, we use the finite element method to analyze the stability of a Ag/BSCCO superconducting tape. The equations governing the entire system are Maxwell's equations and:

$$\nabla \bullet (k(T)\nabla T) + E \bullet J + Q_{ext} = C(T)\partial T/\partial t \quad (1)$$

where $k(T)$ is the temperature dependent thermal conductivity, E is the induced electric field, J is the current density, $C(T)$ is the temperature dependent specific heat and Q_{ext} is any external heat source (e.g. a crack in epoxy). The most general case of a high-T_c tape conductor is shown in Figure 1. In the superconductor, the electric field is exponentially increasing with respect to the ratio of the current in the superconductor, I_{sc}, and the critical current, I_c:

$$E_{sc} = E_c(I_{sc}/I_c)^n \quad (2)$$

where E_c is the critical electric field that determines I_c and n is the index of transition (a higher n-value corresponds to a sharper transition from the superconducting state to the normal state). In the

Ag the electric field is determined by Ohm's Law:

$$E_{Ag} = \rho_{Ag}I_{Ag}/A_{Ag} \quad (3)$$

where ρ_{Ag}, I_{Ag} and A_{Ag} are the resistivity, current and cross-sectional area of the Ag, respectively. By knowing the total operating current, $I_{op} = I_{sc} + I_{Ag}$, and that the electric field must be constant across any x-y plane, E_f - E_{sc} = E_{Ag}, I_{sc}, I_{Ag} and E_f are determined.

Starting with the tape at steady-state with a current I_{op} operating in a magnetic field B, a heat pulse is introduced to drive the tape normal locally. The tape is considered unstable when the temperature rises such that E_f does not vanish and the tape does not return to the initial state. The magnitude of the pulse required to cause the tape to become critically unstable is determined and the values at various fields ranging from 0 to 20 T are calculated.

The results for a planar source in the Ag that is 1.6 mm long in the center of a 20.2 mm section of tape for $I_{op}/I_c = 0.75$ at 4.2 and 20 K have been determined and are shown in Figure 2. For the 4.2
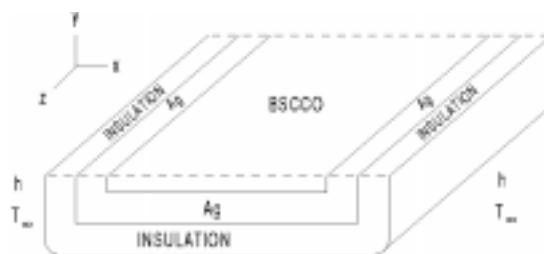

Figure 1.   One-half cross-section of a Ag/BSCCO superconducting composite tape.
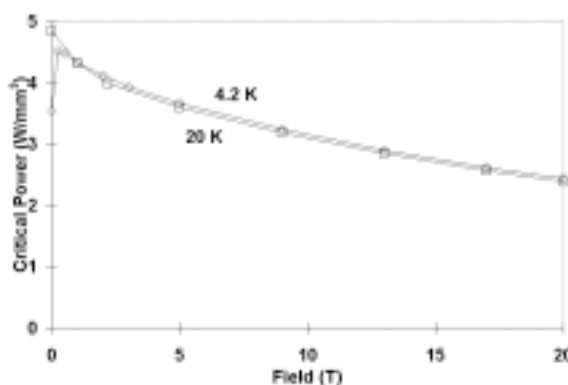

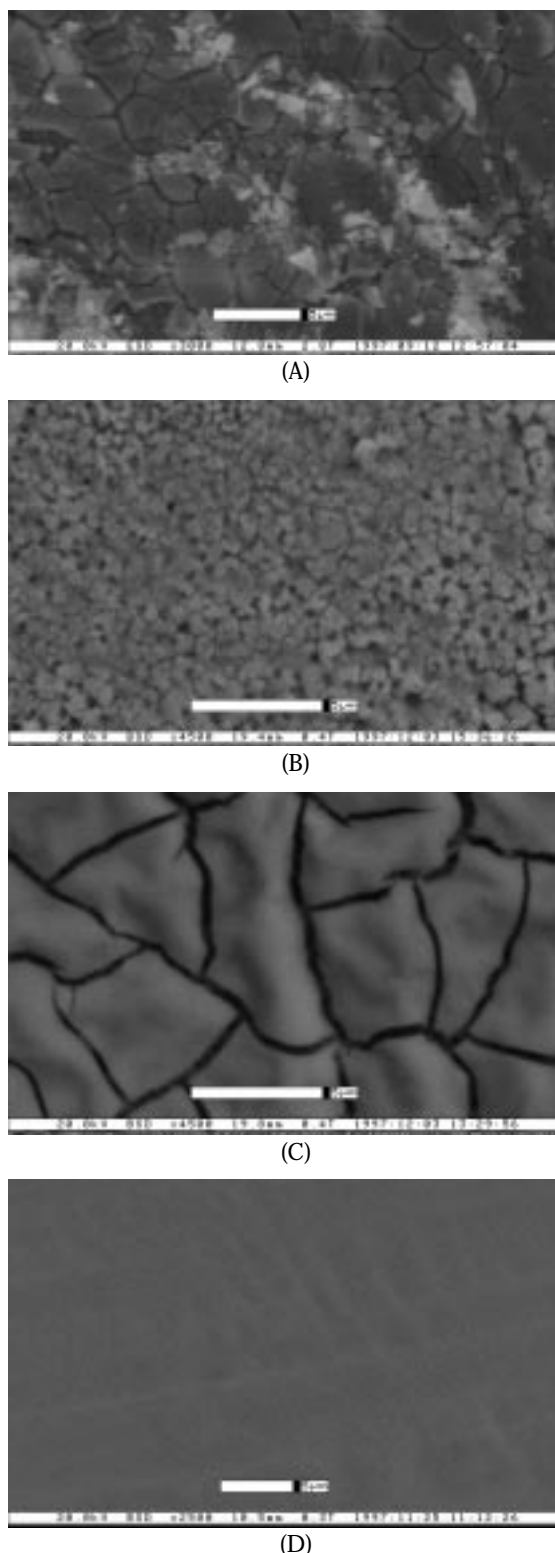**Figure 2.**   Critical power for a 1.6 mm long planar source in the BSCCO.

K case, the critical power increases at low fields. In these cases, the critical current falls below the operating current. For all other cases, the critical power decreases as the field increases and the quench occurs as a result of exceeding the critical temperature.

Sol-Gel CeO$_2$ as Buffer Layer for Surface Coated YBCO Superconductor on Ni Substrate

Celik, E., NHMFL and Sakarya Univ., Turkey, Metallurgy
Hascicek, Y.S., NHMFL

CeO$_2$ film with cubic fluorite structure and good thermal expansion match is generally used as one of the best buffer layer and this material reduce the lattice mismatch between Ni and YBCO.[1] Various vacuum methods have been used for preparation of CeO$_2$ buffer layers. The sol-gel process offers a new possibility to synthesis oxide layers by applying liquid precursors to substrate by dipping, spinning, or spraying. Our objective is to produce CeO$_2$ buffer layer on Ni substrate via sol-gel method.

The deposition of sol-gel thin films consists of three steps. First, fluid sols were prepared from cerium (IV) nitrate, cerium (IV) ammonium nitrate, cerium (III) 2,4 pentanedionate and colloidal CeO$_2$ in H$_2$O based precursor materials. The second stage was dipping of polished Ni substrate into these sols. The final stage was heat treatment for drying and oxidizing. The heat treatment was at 450 °C for 1 hour. XRD and DTA measurements show that CeO$_2$ formation starts at 420 °C. Figure 1 shows typical surfaces of CeO$_2$ thin films produced from four different solutions. It was found that different anions and their amounts influence the structure of films. As seen in Figure 1 as a buffer layer, solutions A, B, and C are not acceptable, but D seems to give a very smooth surface. Once we optimize the sol-gel process on polycrystalline Ni substrate, textured Ni substrate will be coated with CeO$_2$ for non-vacuum surface coated YBCO conductor development.

(A)

(B)

(C)

(D)

Figure 1. Typical SEM micrographs of surfaces of CeO$_2$ buffer layers produced by sol-gel process from four different solutions: A, B, C, and D.

References:

[1]   Hirai, M., *et.al.*, Jpn. J. Appl. Phys., **33**, 5219-5222 (1994).

# Axial Characteristics of Composite Test Coils at 4.2 K

Dixon, I.R., NHMFL
Markiewicz, W.D., NHMFL
Marshall, W.S., NHMFL

Introduction. From thermal and quench loading, axial tensile stress may develop in some coils and reinforcement sections of the 900 MHz NMR magnet. The tensile stress may cause each turn of conductor to separate from one another, leading to epoxy to conductor bond failure. The limitations of these composite cylinders, however, are not fully understood and data is not available in the literature. Therefore the axial properties of small coils as influenced by their electrical insulation are characterized. Sample coils consisting of two conductor layers are manufactured and loaded in tension along their axis to measure ultimate strength and modulus at 4.2 K.

Special support fixtures are developed to support the sample for test. The test fixtures provided a means of holding the samples through their wall thickness. The fixtures supported the inner diameter of the sample while pressing the outer diameter with compression tabs. An illustration of the support fixture is shown in Figure 1.
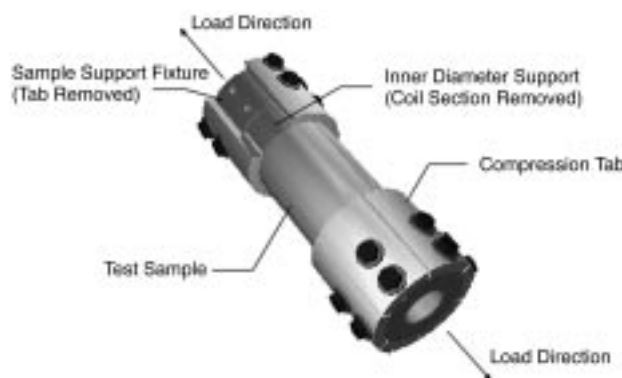
Figure 1.   Support fixture for axial measurement of superconducting coils.

Three types of samples have been measured and are reported. Each test specimen is a two layer coil with a nominal 50.5 mm inner diameter and 127 mm length. Nb_3Sn and NbTi conductors are used, however the Nb_3Sn conductors are not reacted. Glass cloth is added to the inner, mid, and outer layers of the coils. Table 1 contains information detailing each type of sample tested. Four samples of each type are manufactured.

Table 1.   Characteristics of axial test cylinders.

	Type 1	Type 2	Type 3
Conductor	Nb_3Sn	NbTi	Nb_3Sn Soldered
Conductor Dimension	1.04 mm x 2.08 mm	1.25 mm x 2.26 mm	1.40 mm x 2.16 mm
Insulation	E-Glass	Formvar	Polyester
Cloth	S2-Glass	E-Glass	E-Glass

Mechanical Measurement Results. Tables 2 and 3 summarize the ultimate strengths and moduli for each sample. Two strain gages were attached on opposing sides for modulus measurements. The maximum tensile stress that exists in the 900 MHz NMR magnet occurs in the reinforcement of coil 7 during quench. The stress is 20 MPa, below all ultimate strengths measured in this test series. Two values of modulus are given for the polyester samples. The first column are those determined from the tensile tests and the second are determined from compressive tests.

Table 2.   Summary of ultimate strengths of axial cylinder tests at 4.2 K, units in MPa.

Sample	E-Glass Nb_3Sn	Formvar NbTi	Polyester Soldered
A	55.2	50.3	35.8
B	67.0	54.1	38.3
C	66.1	51.4	55.5
D	48.0	43.1	58.8
Average	59.1	49.7	47.1

Table 3. Summary of Young's modulus of axial cylinder tests at 4.2 K, units in GPa.

Sample	E-Glass Nb$_3$Sn	Formvar NbTi	Polyester (Tension)	Polyester (Comp.)
A	62.2	65.0	8.4	
B	63.0	68.8	5.7	
C	67.4	68.7	7.2	25.5
D	66.3	72.2	7.5	21.6
Average	64.7	67.7	7.2	23.6

# Computation of Radial Offsetting Force Distribution Along Axis of Solenoids

Dixon, I.R., NHMFL
Eyssa, Y., NHMFL
Markiewicz, W.D., NHMFL

Introduction. Computation of the radial forces produced on a single coil offset a prescribed radial displacement with respect to the central axis of all other remaining coils is derived. The solution allows the use of a 2-D analysis for computation of the magnetic fields and gives the displacing force due to an offset as a function of axial position. The loads from a 1 mm radial offset on coil 5 of the 900 MHz NMR magnet is presented.

The formulation of the force may be illustrated by the distribution of the axial field. With coils centered, the axial field at an axial position z around the circumference of a coil is equal. However, with a prescribed displacement u the field profile changes and the field distribution may be pictured as shown in Figure 1.
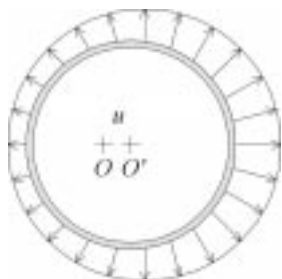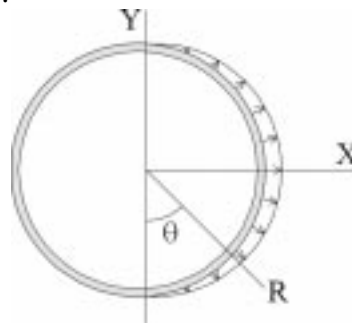

Figure 1. Magnitude of axial field with coil offset a displacement u.

The difference in axial field is obtained by subtracting the axial field of the left side from the right side. This difference is assumed to have a sinusoidal distribution as

$$B_Z^R(\theta) = A \sin\theta \qquad (1)$$

Where A is the difference in the axial field at $\theta = \pi/2$. A schematic of the net axial field is shown in Figure 2.

Figure 2. Net axial field profile with coil offset.

The axial field in radial coordinates is expressed in Cartesian coordinates by

$$B_Z^Y(\theta) = A \sin\theta \cos\theta \qquad (2)$$

$$B_Z^X(\theta) = A \sin^2\theta \qquad (3)$$

The force is expressed as

$$F = \int_0^l i\, B\, dl = \int_0^{\pi R} iB_Z^R\, d\theta \qquad (4)$$

The force component integrates to zero and the force component, F_X becomes

$$F_X = \int_0^{\pi R} iA \sin^2\theta \, d\theta \qquad (5)$$

$$F_x = iA \left[\frac{\theta}{2} - \frac{1}{4}\sin 2\theta \right]_0^{\pi R} = \frac{i\, \pi AR}{2} \qquad (6)$$

The offset force, F_X, is approximated by the 2-D solution of the axial field of a coil shifted $+u$ and $-u$ to determine the parameter A. The positive displacement represents the leading edge of the coil offset and the negative displacement represents the trailing edge of the coil offset.

Results. As an example, the largest Nb$_3$Sn coil of the 900 MHz NMR magnet is used to illustrate a radial offset force distribution. Figure 3 shows the distribution of radial force per unit mm along the length of the coil for a 1 mm radial offset.
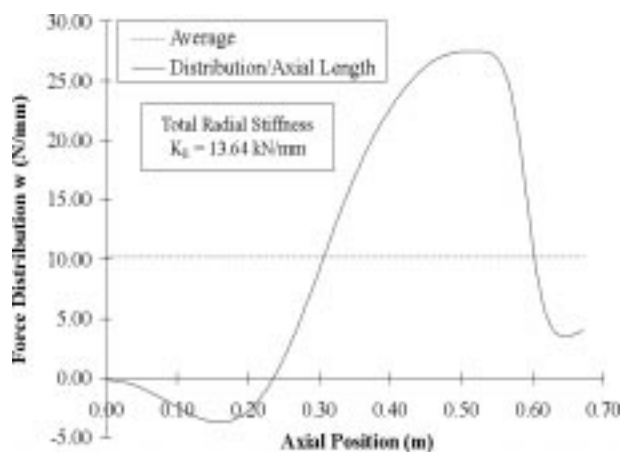

Figure 3. Radial offset force of coil 5 per unit length, prescribed displacement of 1.0 mm.

Resistive and Superconducting Magnet Configurations for Levitation of Weakly Diamagnetic Materials

Eyssa, Y.M., NHMFL
Schneider-Muntau, H.J., NHMFL

The magnetic fields that can be generated today by superconducting and resistive magnets are so strong that even weakly diamagnetic materials can be levitated. Materials with magnetic susceptibilities in the order of 10^{-5} require a product of field times field gradient of about 1000 T^2/m. Such values are easily obtained in standard 12 to 20 T, 30 to 50 mm bore resistive and superconducting solenoid magnets. To levitate larger objects, magnets with wider bores and different field configurations than solenoids are necessary, as for instance a split coil magnet with opposite field direction in the two halves (Figure 1). In this study, we characterize the levitation capability of some of the resistive magnets. The levitation results from a balance between the
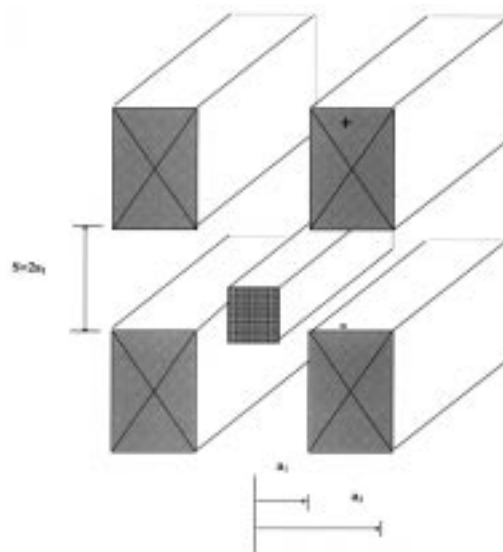
Figure 1. Levitation in a split Helmholtz race-track magnet.

magnetic force, Fm, acting on every molecule in the levitated specimen, and the gravitational force. Diamagnetism is a general attribute of matter, in a few materials it is covered by additional para- or ferromagnetism. The molecular diamagnetism is caused by electrons adjusting their orbits to reduce their energy in the presence of an external magnetic field. These magnetic levitation forces are many orders of magnitude weaker than forces on ferromagnetic materials.

An object will levitate when its magnetic force balances the gravitational force. The magnetic force per unit volume is related to the field and field gradient as, $\vec{F} = x\,(B.\nabla)\,\vec{B}$, where x is the magnetic susceptibility, and $\vec{B}$ is the magnetic field vector. In a solenoidal cylindrical coordinate system the total axial and radial forces, F_r and F_z, integrated over the levitation volume V are,

$$F_r = x \iiint [B_z \frac{dB_z}{dr} + Br \frac{dB_r}{dr}]dv \quad F_z = x \iiint B_z \frac{dB_z}{dz} + B_r \frac{dB_z}{dr}]dv$$

The radial force averages to zero and is self stabilizing. The axial balancing force is dominated by the *Bz (dBz/dz)* term and is more uniform for a specimen with a radius small compared to the levitation solenoid bore. Equating the axial force with the gravitational force, Fg = ρgV, results in a relation between the magnetic susceptibility, the magnet field, bore, configuration, the specific gravity ρ and the levitated object volume V. In case of a superconducting magnet, it is convenient to

correlate that relation to the maximum winding field, Bmax, since it is the quantity that determines the superconducting current density. Bmax in a single solenoid system occurs at the inner radius on the mid-plane. In case of a resistive magnet, it is natural to correlate the levitation relation to the power consumption of the magnet. By equating the gravitational and levitation axial forces the lower bound on the magnetic susceptibility x that can be levitated as function of the maximum field or dissipated power W is,

$$x \geq \frac{\rho g}{\lambda_{B_{max}}} \frac{a_1}{B_{max}^2}, \ or \ \ x \geq \frac{\rho g}{\lambda_w} \frac{\rho_e a_1^2}{p_f W},$$

where ρ_e is the conductor electrical resistivity and p_f is a filling factor. The levitation factor λ is a dimensionless constant that relates to bore diameter, magnet geometry, to field or power. It is a geometry factor, like the Fabry factor, that defines the optimum magnet geometry and allows for a comparison between different magnet designs. We have computed the levitation factor for several solenoidal and racetrack geometries. Figure 2 shows the power related l factor for a single solenoid system. In our 50 mm magnet we can levitate diamagnetic materials with $x = 0.5 \times 10^{-5}$ and higher, while in our 200 mm bore x has to be higher than 1.0×10^{-5}.
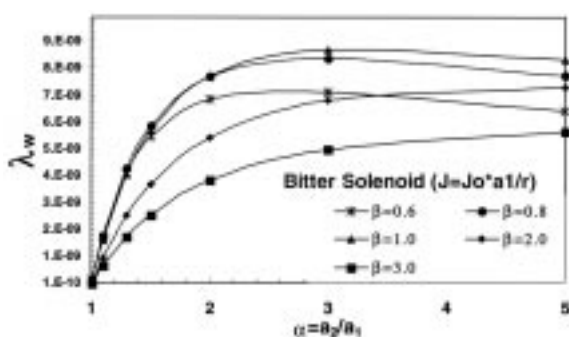
Figure 2. Levitation factor for resistive single coil relative to power consumption, W.

Conclusion. Magnets with small bore diameters have strong gradients. The condition of levitation of diamagnetic matter is, therefore, easy to achieve for small objects. Large bore magnets have lower gradients. To achieve the same B x grad B product the field must be increased. Today's conductor materials set limits on the achievable fields that restrict the object size to about 100 mm diameter for

superconducting magnets and to 180 mm diameter for a 20 MW resistive magnet. Large objects would require higher power consumption or unavailable higher field materials in case of superconducting magnets. For example to levitate a human body only resistive magnet in a racetrack configuration could satisfy the field and the volume requirements. A field of almost 40 T is needed, and the continuous power demand would be about 1 GW.

High Temperature Superconducting Shim Coil Insert for Improved Homogeneity of the 20 T Oxford Low Temperature Superconducting Magnet

Hascicek, Y.S., NHMFL
Kuhns, P., NHMFL
Godfrey, M.I., NHMFL
Weijers, H.W., NHMFL
Eyssa, Y., NHMFL
Van Sciver, S.W., NHMFL
Moulton, W., NHMFL
Schneider-Muntau, H.J., NHMFL
Dai, W., Oxford Superconductor Technologies
Cowey, L., Oxford Superconductor Technologies
Marken, K.R., Oxford Superconductor Technologies

High magnetic field homogeneity is necessary for many experiments like high resolution NMR for organic materials and solutions. The present homogeneity for the Oxford 20 T magnet at NHMFL is about 150 ppm across 5 mm DSV.[1] This level is not sufficient for resolving chemical shifts on the order of a proton. Since the upper critical fields of HTS are very high it is possible to build small compact HTS shim coils which can be placed in the bore of the magnet and cause no heating and in turn no additional liquid helium consumption. Calculations show that by using two pairs of pancake coils in the bore of the 20 T Oxford superconducting magnet we can improve the homogeneity by more than an order of magnitude.

The short sample tests, from the conductor received from OST, showed an I_c of 230 A (J_{ce}=187.3 A/mm^2) at 4.2 K and at self field. This value was about 77 A (62 A/mm^2) at 4.2 K and 17 T. Also, a single pancake was built and tested to verify the long length performance. That pancake had an I_c of 160 A at 4.2 K and self field. Our experience shows that the I_c of such a coil at 17 T and 4.2 K should be about the half of the self field value. Once the conductor proved to meet the specifications of the design one double and four single pancakes were fabricated with wind-and-react (W&R) technology using ZrO_2 spray insulation. The central double pancake coil has 48 turns, 21 mm ID, 45 mm OD, 7.5 mm height and 2 mm split. This central double pancake was a jointless one. The outer pancakes have 2x25 turns, 21 mm ID, 45 mm OD, 9 mm split and 14 mm height. The outer pancakes are joined by soldering already reacted Bi-2212/Ag tape conductor. Current leads from the pancakes are also stacked HTS tape conductors. No reinforcement was necessary considering the stress capability of the conductor, expected background fields and operating current densities. Stress dependence of I_c was actually tested by a novel In-situ Lorentz Force Straining[2,3] experiment at a background field of 30 T.

The coils were assembled on a Variable Temperature Insert (VTI), which accepts an NMR probe to verify the homogeneity with and without the HTS shim coils. The height of the variable insert was made adjustable to center the shims and the background magnet. Therefore, there was no need to mount the gradient coils on. Figure 1 shows the lower part of the VTI together with the HTS shim coils.
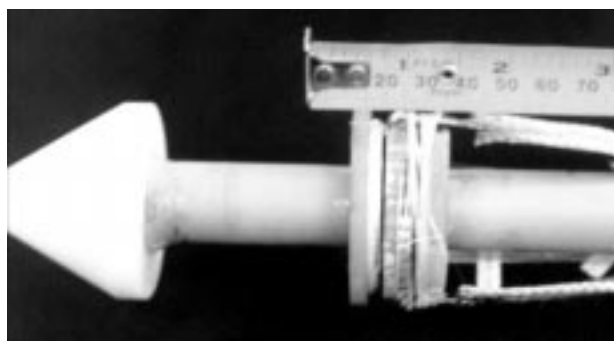

Figure 1. Bottom of VTI together with the HTS shim coils.

The proton NMR measurements showed that the homogeneity of the background field was worse than 150 ppm. It also turned out that a very small misalignment of the shim coils and background magnet can have serious effects when one is looking for few ppm homogeneity. The best homogeneity achieved was about 50 ppm with the HTS shim coils. All the coils exceeded the design critical currents, and performed very well despite the fact that we had to repeatedly thermally cycle them several times exposing the coils each time to the atmospheric humidity. Not only that the coils were mounted and dismounted few times because of a cold leak and other unforeseen reasons!!!

An HTS shim coil insert which consisted of two pairs of pancake coils was built by using W&R process from Bi-2212/Ag tape conductors. They were assembled on a VTI. All the coils exceeded their design currents. Proton and lidium NMR measurements showed that the best homogeneity achieved was about 30 ppm with the HTS shim coils.

References:

1   Kuhns, P., *et al.*, NHMFL internal report (1994).
2   US patent application pending.
3   Hascicek, Y.S., *et al.*, NHMFL Annual Report 1996, p 168.

High Field Critical Currents in Nb47w%Ti Multifilamentary Composites

Hong, S., Oxford Instruments, Inc.
Hentges, R., Oxford Instruments, Inc.
Marken, K., Oxford Instruments, Inc.
Zhang, Y., Oxford Instruments, Inc.

Composites with various volume fractions of Nb47w%Ti were tested for critical current values in fields up to 13 T at 2.2 K. Test samples included 7:1, 1.35:1, and 1:1 copper to non-copper ratios in rectangle configurations. The purpose of the investigation was to understand the effect of heat

treatments and processing on the current density of these wire types.

Current densities were measured at 0.1 μv/cm. Results show that the processing of this wire yielded J_c values averaging 105 A/mm^2 at 13 T when measured at 2.2 K. The field shift in this region was found to be approximately 2.5 T from 4.2 K to 2.2 K.

Wire of this type is being used in conjunction with bronze processed Nb_3Sn to build NMR spectroscopy magnets operating at 2.2 K and 800 MHz.

Nb_3Al and $Nb_3(Al,Ge)$ Multifilamentary Conductors Fabricated by Continuous Rapid-Heating/Quenching Process

Iijima, Y., National Research Institute for Metals (NRIM), Tsukuba, Japan
Inoue, K., NRIM
Kosuge, M., NRIM
Takeuchi, T., NRIM
Yuyama, M., NRIM
Sato, A., NRIM

Recently we developed a new fabrication process, a continuous rapid-heating/quenching process, for Nb_3Al multifilamentary wire, which showed two to five times larger non-Cu J_c (4.2 K) in fields from 0 to 26 T than those of commercially available superconducting wires. In this process, a multifilamentary composite wire, composed of Nb matrix and Nb/Al micro-composite cores, was rapidly heated up to about 2000 °C and then quenched into a molten Ga bath. The highest H_{c2} obtained for the Nb_3Al conductor was 26.3 T at 4.2 K and 29.1 T at 1.8 K. The newly developed Nb_3Al multifilamentary conductor should be commercialized and take the place of Nb_3Sn conductor in near future.

By the way, Ge addition to Nb_3Al is well known to improve not only T_c but also H_{c2} (4.2 K). Therefore, we tried to apply the new process to the fabrication of $Nb_3(Al,Ge)$ multifilamentary conductors. An Al-20at%Ge alloy rod was used as a starting material. By using a rod-in-tube process, we fabricated a multifilamentary composite wire, composed of Nb matrix and Nb/Al-20at%Ge micro-composite core, which was rapidly heated up to about 2000 °C and then quenched into a molten Ga bath. Although Nb-Al super-saturated bcc phase filaments are ordinarily formed in the beginning of the rapid-heating/quenching process of the Nb_3Al multifilamentary wire production, the Ge addition prevented the formation of the supersaturated bcc phase, resulting in the formation of $Nb_3(Al,Ge)$ filaments with disordered A15 crystal structure. However, additional annealing at 700 °C to 900 °C improved the long-range ordering of the $Nb_3(Al,Ge)$ crystal structure, and increased T_c from 15.3 K to 19.4 K and H_{c2}(4.2 K) from 20 T to above 33 T. The H_{c2} values were measured by a resistive method in gradually increasing fields. The J_c(4.2 K) of $Nb_3(Al,Ge)$ multifilamentary wire is relatively low in the fields lower than 18 T, but not so low in the fields above 20 T. J_c (4.2 K) over 100 A/mm^2 were obtained for the $Nb_3(Al,Ge)$ multifilamentary conductors in fields around 25 T, which is the highest value reported up to date for superconductors with the multifilamentary structure, which is the most preferable structure for the practical use. The maximum H_{c2}(4.2 K), estimated from a Kramer plot, was 39.4 T, which is a little lower than that of an arc-melted $Nb_3(Al,Ge)$, i.e. 40 T, but much higher than those of the commercialized $(Nb,Ti)_3Sn$ multifilamentary wire, i.e. 24 T to 26 T.

Influence of a SnI$_4$ Coating of YBCO Grains on the Formation of a Uniaxial Texture

Kugeler, O., NHMFL/RWTH, Aachen, Germany
Hascicek, Y., NHMFL

Aiming at a *non-vacuum* technique for the large-scale fabrication of YBCO, one has to find alternative ways to obtain a texture in the material. A promising method utilizes the coating of YBCO grains with a layer of tin(IV)iodide.[1]

Commercial YBCO powder (mesh 5 μm) was submitted into a solution of tin(IV)iodide in acetone and stirred until the acetone completely evaporated. This process yielded SnI$_4$ coated YBCO grains at an overall weight ratio of 1:12. DTA measurements of the coated powders revealed a reaction between SnI$_4$ and YBa$_2$Cu$_3$O$_{7-\delta}$ upon heating, at temperatures of about 370 °C, indicated by the exothermal peak in Figure 1. This peak is slightly higher than the characteristic boiling-peak of SnI$_4$ at 364.5 °C. Melting of the SnI$_4$ coated YBCO starts at onset temperatures around 900 °C, which is far below the peritectic temperature of pure YBCO (1015 °C). Bulk samples were prepared from SnI$_4$ coated and phase pure precursors and heat treated—under identical processing conditions—at temperatures below 980 °C for durations below an hour. The micrograph of the sample made from the uncoated precursor shows the typical sintering structure, reflecting the original shape of the precursor powder, (Figure 2). In samples of the coated precursors liquid phase formation occurred at the grain boundaries (Figure 3), which hints at a significant change in the phase diagram of the YBCO system towards lower temperatures. This is most probably caused by the iodide additions. In future work we will determine to what extent changes in the phase diagram can be utilized to improve the texture in the material and if alternative substrate materials, like silver-tape or ceria coated nickel tape, which is concurrently developed in our group, can be used.
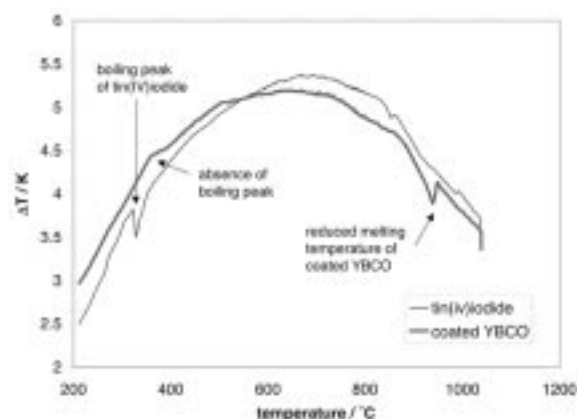
Figure 1. DTA curves of pure tin(iv)iodide and YBCO powder coated with tin(IV)iodide. The melting peak of SnI$_4$ is missing in the coated powder—instead an exothermal reaction occurs.
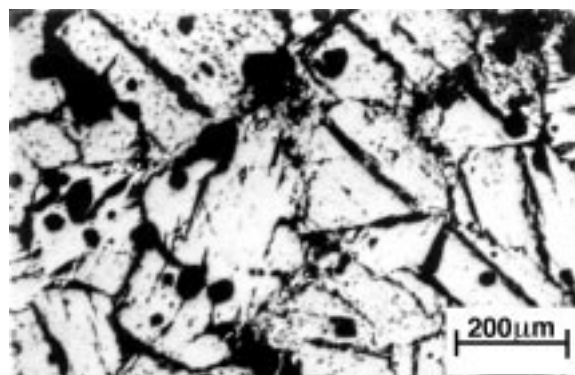
Figure 2. Horizontal cross section of YBCO powder sintered at 980 °C.
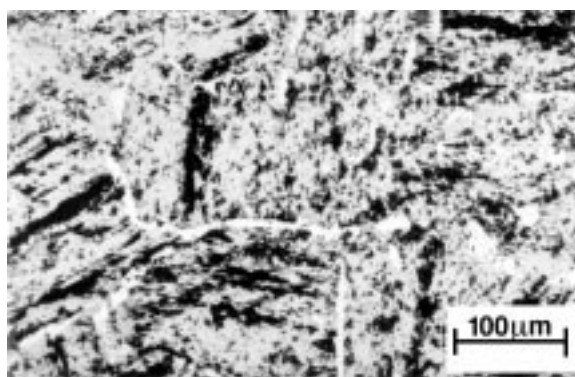
Figure 3. Horizontal cross section of coated powder heat-treated at 980 °C, note the formation of liquid phase at the grain boundaries.

References:

1. Zheng, X.-G., *et al.*, Supercond. Sci. Technol., **9**, 5, 358 (1996).

Characterization of the Critical Current of Cable-In-Conduit Conductors with Nb₃Sn Strands under the Mechanical Strains Typical of Magnet Operation

Miller, J.R., NHMFL
Walsh, R.P., NHMFL
Haslow, M.R., NHMFL
Kenney, W.J., NHMFL
Miller, G.E., NHMFL

With the extremely high peak fields in which superconducting coils for the 45 T Hybrid must operate (the two innermost subcoils contain strain-sensitive Nb_3Sn superconductor and experience peak fields of 17 and 13 T, respectively), it is essential to account for the total intrinsic filament strain resulting from the combination of differential contractions during cooldown from the reaction temperature as well as the hoop and axial loading of conductors during energization of the magnet. We have examined this problem through tests of specially constructed model cable-in-conduit conductors (CiCCs), wherein the NHMFL split-solenoid was used to measure critical currents in excess of 10 kA, at fields up to 14 T, and with applied longitudinal loads up to 250 kN. Model conductor tests are supplemented by critical-current vs. applied-strain measurements on single wires, and data were correlated using a relation of the form:

$J_c(B,T,\varepsilon) = C(e) \, [B_{c2}(T, \varepsilon)]^{-1/2} \, (1 - t^2)^2 \, b^{-1/2} \, (1 - b)^2$,

where:

$$t = T/T_{c0}(\varepsilon), \ b = B/B_{c2}(T,\varepsilon),$$
$$B_{c2}(T, \varepsilon) = B_{c20}(\varepsilon) \, (1 - t^2) \, [1 - 0.31 \, t^2 \, (1 - 1.77 \ln t)],$$
$$B_{c20}(\varepsilon) = B_{c20m} \, (1 - a<\varepsilon>^{1.7}),$$
$$T_{c0}(\varepsilon) = T_{c0m} \, (1 - a<\varepsilon>^{1.7})^{1/3}, \text{ and}$$
$$C(\varepsilon) = C_0 \, (1 - a<\varepsilon>^{1.7})^{1/2}.$$

B_{c20m} and T_{c0m} are the maximum values of upper critical field and critical temperature (corresponding to zero intrinsic strain and either zero temperature or zero field, respectively), C_0 is the pinning parameter, and a is the strain sensitivity

parameter. This relation differs from previous versions in the literature by its use of $<\varepsilon>$, where:

$<\varepsilon> = ((2/3) \, [(\varepsilon_1 - \varepsilon_2)^2 + (\varepsilon_2 - \varepsilon_3)^2 + (\varepsilon_3 - \varepsilon_1)^2]^{1/2}$,

where ε_1, ε_2, and ε_3 are the principle strains. For longitudinal loading of a cylindrically symmetric, isotropic medium, the principal strains are ε_Z, ε_R, and ε_Θ, respectively, and are given by the following:

$\varepsilon_Z = \sigma_Z/E$,

$\varepsilon_R = \varepsilon_\Theta = -\nu \, \varepsilon_Z$,

where σ_Z is the longitudinal, applied stress, E is the Young's modulus for the medium, and ν is its Poisson's ratio. This form is desirable for characterizing the behavior of large CiCCs because it includes multidimensional strain effects. We propose that the typically observed asymmetric character of critical current vs. intrinsic strain of Nb_3Sn conductors can be understood in this formalism by noting that the Poisson's ratio of the matrix, the dominate fraction of material in all multifilamentary-Nb_3Sn wires, must show a variation from about 0.37 in the elastic region to about 0.5 in the plastic region. This shift quite likely occurs gradually as a function of strain and is probably centered near 0.3 % strain.

Using the above formalism in conjunction with single-wire tests, the number of free parameters for fitting data taken on CiCC model conductors. A variety of conductors have been tested. Figure 1 shows a fit to typical data taken on a CiCC model conductor heat treated along with Coil B of the
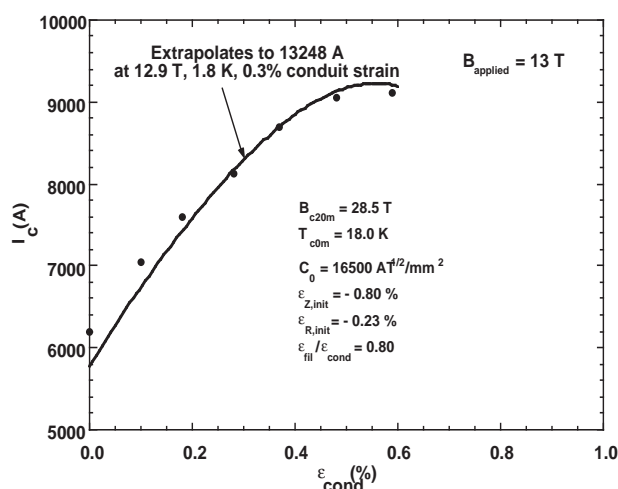
Figure 1. Critical current vs. strain applied to the conduit of a heat-treatment witness model of the Coil-B CICC.

Hybrid outsert. A fit was possible only by accounting for initial compressive strains in both the longitudinal and transverse directions as well as a deamplification factor for filament strain vs. conduit strain. All are reasonable in view of the CiCC composition and its history of processing.

QUench Initiation and Propagation Studies (QUIPS) with Conductors Relevant to the Superconducting Outsert of the 45 T Hybrid

Miller, J.R., NHMFL
Amemiya, N., Yokohama National Univ., Electrical and Computer Engineering
Haslow, M.R., NHMFL
Kenney, W.J., NHMFL
Miller, G.E., NHMFL
Prestemon, S.O., NHMFL
Windham, C.L., NHMFL

Experimental studies of quench initiation and propagation on a large scale are difficult because large-scale conductors are expensive to fabricate and there are few facilities where an appropriately long test conductor can be exposed to uniform and sufficiently high field that the test is relevant. For example, in addition to having similar geometry and composition, the conductor should be tested with a similar stabilizer current density and with a similar current-sharing temperature margin.

The innermost coil of the 45 T Hybrid outsert uses a Cable-in-Conduit Conductor (CiCC) made with Cu/Nb_3Sn composite wires and is designed to operate at 11 kA with a maximum field of nearly 17 T. It will be cooled by HeII at 1.8 K and 1 bar. To have a relevant test, one would normally expect to have to reproduce these current, field, and temperature conditions with some fidelity. However, the field is really only necessary in that, for a particular operating current, it determines the current-sharing temperature margin. Fortuitously,

the unreacted conductor for the innermost outsert coil contains a superconductor (Nb-1wt%Ti) that has a zero-field critical temperature of approximately 9 K and a zero-temperature critical field of approximately 1.4 T. Thus, a section of this unreacted conductor carries 11 kA at 1.8 K in its own self field, and it has a similar temperature margin as the reacted conductor at 11 kA, 1.8 K, and 17 T. Therefore, tests of the unreacted conductor with zero applied field can provide a very relevant benchmark of the analyses performed with complex computer codes that model the behavior of CiCCs.

A bifilar winding containing approximately 49 m of conductor was produced and instrumented with an array of voltage taps, pressure taps, and heaters for this test. The construction and composition of the unreacted test conductor are listed in Table 1. Typical data from the voltage taps during initial tests are illustrated in Figure 1.

From such data, along with a careful characterization of the superconducting and thermophysical properties of the conductor, we deduce normal front propagation as well as

Table 1. Construction and composition of the test conductor.

Unreacted Coil-A Conductor	
Cable pattern	5 x 5 x 3 x (6 Nb_3Sn comp. + 1 Cu wires, 0.433-mm dia.)
Transposition lengths (mm):	
4th stage	284
3rd stage	159
2nd stage	77
1st stage	19
wire	9.5
Composition:	
A_{cond} (mm^2)	79.44 (65.82 - Cu*, 7.97 - Nb-1wt%Ti, 5.65 - Sn)
	50.30
A_{He} (mm^2)	82.71
A_{steel} (mm^2)	(80.20 - wall, 2.51 - foil wrap)
	41.32
$A_{insulation}$ (mm^2)	

* Includes copper both inside and outside the barrier
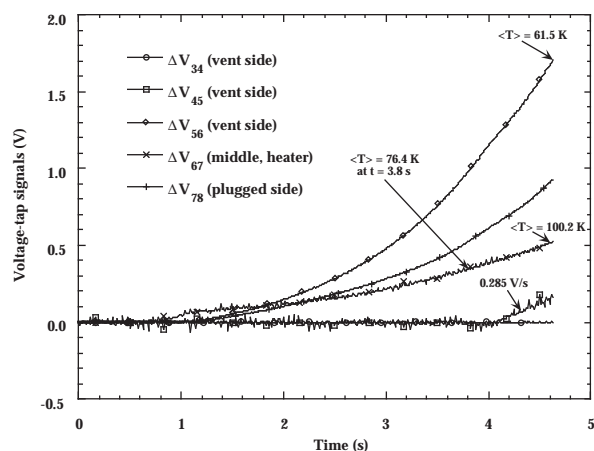
Figure 1. Development of voltages along the conductor due to a quench starting from the central zone.

temperature and pressure evolution in the quenched zone for comparison with computer-code analyses. For example, data of Figure 1 correspond to normal-front velocities that range from approximately 1 m/s early in the quench to 4 m/s late. The calculated values for the same operating conditions were much smaller— approximately 1/5 the measured value at one point in time—neither did they grow at the observed rate. Work is continuing on both the tests and the computer model to sort out the discrepancies.

ESEM Hot Stage Evaluation of Sol-Gel Insulation Coatings for High Field High Temperature Superconducting Magnets

Mutlu, I., NHMFL and Harran Univ., Turkey, Physics
Goddard, H.R.E., NHMFL
Hascicek, Y.S., NHMFL

High temperature, thin ceramic insulation coatings are necessary for the application of high temperature superconductors (HTS) in high field magnet technology. Especially in the so called "wind and react" technology, insulation coatings have to withstand the final heat treatment at about 900˚C, otherwise turn-to-turn insulation will be broken. We have developed a sol-gel coating method for HTS tape conductors at NHMFL.

The ZrO_2 coatings were obtained by dipping the silver sheathed HTS tape in a solution of an organozirconium. The microstructure of the insulator on the tape was studied between room temperature and 600 °C using an environmental scanning electron microscope (ESEM) equipped with a hot stage. BSCCO/Ag tape (2 mm x 2 mm) was dipped into solution and then put in the hot stage of ESEM. As the coated tape sample heated microstructural changes were observed and recorded. Gelling and cracking must start as soon as the sample is withdrawn from the sol, since the cracks were always present in the coating even before we started heating. As the temperature increases the cracks grow in width and islands shrink in size. The process of shrinkage begins around 200 °C and continues until approximately 600 °C. Although the tape surface looked as if covered with islands of insulation starting at about 300 °C there was no flaking, indicating very good bonding. Figure 1 shows the crack and island morphology starting from room temperature to
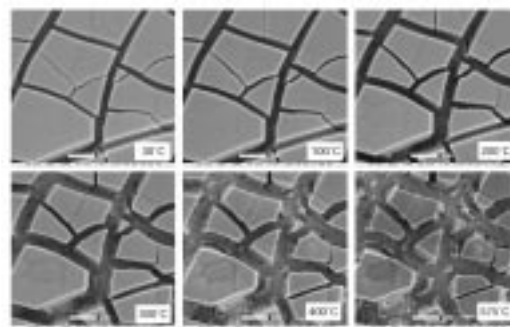
Figure 1. ESEM micrographs of sol-gel zirconia coating at various temperature as marked. The scale bar in each image is 20 μm. Note that an increased shrinkage in the island size is observed at around 300 °C.
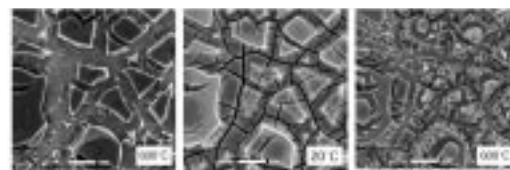
Figure 2. ESEM micrographs of the same area of a tape sample after first and second dipping. The first micrograph on the left is after first dipping at 600 °C, the second and third ones are after second dipping at room temperature and 600 °C as marked. The scale bar is 20 μm.

about 600 °C. The shrinkage is due to organics burning and loss of water while oxide is formed, and it is irreversible. Successive dipping can be used to further thicken the islands and cover the inter island spacing as seen in Figure 2. Figure 2 shows the same area of a tape sample after first and second dipping at room temperature and at about 600 °C. The average coating thickness per dip was about 3 µm.

Sol-Gel Insulation for High Temperature Superconducting Coils

Mutlu, I.H., NHMFL and Harran Univ., Turkey, Physics
Celik, E., NHMFL and Sakarya Univ., Turkey, Metallurgy Engineering
Hascicek, Y.S., NHMFL

We have developed a sol-gel ceramic-based insulation coating process at the NHMFL for providing turn-to-turn electrical insulation for HTS coils.[1] The coatings obtained are compatible with both the high temperatures necessary for processing and the cryogenic temperatures needed for operation. Additionally, they make an excellent insulation from the processing point of view, since zirconia is permeable to oxygen. The sol-gel process is a low temperature chemical route, and the thickness of the coating may be controlled by changing the withdrawal speed and/or the zirconium content in the solution.

Figure 1 shows a typical ESEM micrograph of the insulation layer in a longitudinal section of Ag sheathed powder-in-tube (PIT) Bi -2212 conductor. The presence of cracks is not detrimental as far as this application is concerned. It may actually be advantages due to increased surface area which could improve the mechanical integrity of the finished magnets after epoxy impregnation. Figure 2 shows the surface of sol-gel zirconia coating on HTS tape conductor.
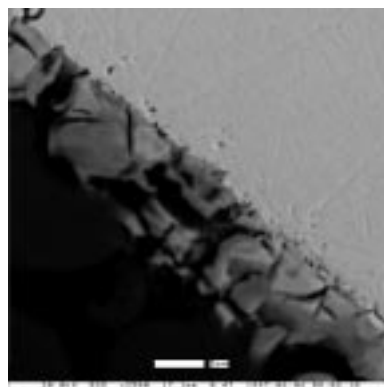
Figure 1. A typical ESEM micrograph of the sol-gel layer. The interface of the coating and silver is well defined and clear. The scale bar is 5 µm.
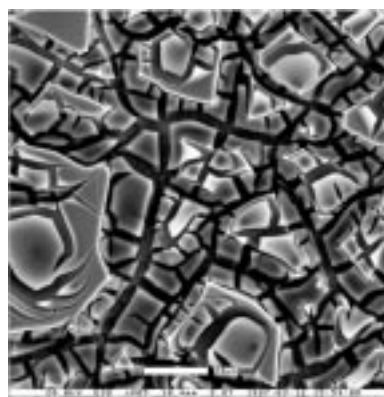
Figure 2. ESEM micrograph of the surface of sol-gel insulation. The scale bars are 20 µm.

Several 15 m lengths of PIT Bi-2212/Ag tape conductors have been insulated and used in double pancake magnet units. These units were heat treated and tested. No shorts were observed, and the stack of six double pancake units produced 1.2 T in a background field of 17.5 T at 4.2K.[2]

This sol-gel insulation process is readily applicable to low temperature superconducting (LTS) magnet applications. In fact, we are in the process of demonstrating the improvement in the packing density one can achieve by using this process in a small Nb_3Sn coil.

References:

[1] Mutlu, I.H. and Hascicek, Y.S., US patent application pending.
[2] Weijers, H.W., *et al.*, CEC/ICMC 1997.

Anisotropic Magnetothermal Conductivity of $Bi_2Sr_2CaCu_2O_x$ Superconductors

Nakamae, S., NHMFL/FSU

Schwartz, J., NHMFL/FAMU-FSU College of
  Engineering

The change in thermal conductivity (κ) of high temperature superconductors (HTS) in a magnetic field is a direct consequence of additional scattering processes between the phonons, the charge carriers and the flux lines. Therefore, knowing magnetothermal conductivity can provide useful information on the nature of heat carriers in HTS and the understanding of the vortex dynamics.

We have measured the in-plane thermal conductivity of a c-axis aligned $Bi_2Sr_2CaCu_2O_x$ superconductor in magnetic fields up to 17 T supplied by the superconducting magnet at the NHMFL. The magnetic field was applied both parallel and perpendicular to the c-axis and always perpendicular to the direction of the heat flow. The results are compared to existing theories. The anisotropy of the in-plane magnetothermal conductivity was also investigated.

The normalized $\kappa(H, T)$ in applied magnetic fields up to 17 T for the two field orientations are presented in Figure 1a and 1b. The theoretical curve shown in Figure 1b is derived from the BRT model.[1] An energy gap of 8 meV produces the best fit curve, though this value is lower than most of the values found in the literature.

The thermal resistance changes (ΔW) in magnetic fields (due to flux lines) are compared to the theoretical values derived from the extended BRT model, which assumes the phononic thermal conductivity to be the main contributor. The results are shown in Figures 2a and 2b. The dotted lines represent the theoretical curves with $f(H/H_{c2})=(H/H_{c2})^{1/2}$ for $H//c$ measurements and $f(H/H_{c2})=H/$

H_{c2} for $H\perp c$ measurements. The $H_{c2}(0K) = 80$ T was used for both calculations. The agreement between the experimental data and the theoretical curves is within 10% for all field values.

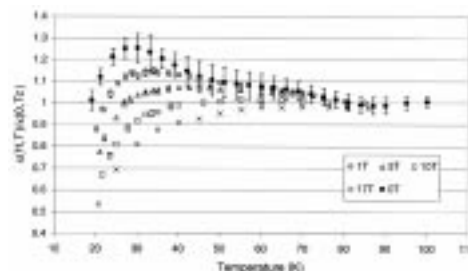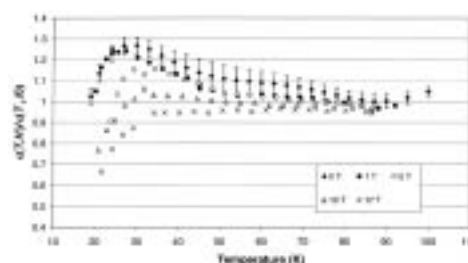**Figure 1a.** Normalized κ (T) for $H//c$-axis.

Figure 1b. Normalized κ (T) for $H\perp c$-axis
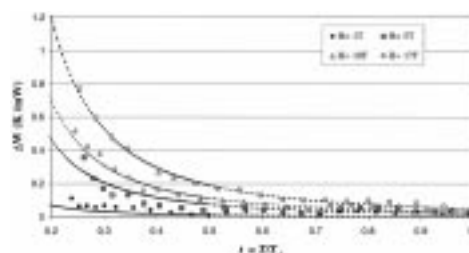

Figure 2a. Thermal resistance change for $H//c$-axis.

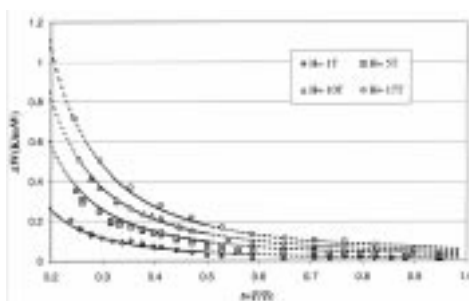**Figure 2b.** Thermal resistance change for $H\perp c$-axis.

References:

[1] Bardeen, J., *et al.*, Physical Review, **113**, 982-994 (1954).

# Recent Progress on Synthesis and Processing of Doped Hg-1223 Superconductors

Sastry, P.V.P.S.S., FAMU-FSU College of Engineering
Amm, K.M., FAMU-FSU College of Engineering
Knoll, D.C., FAMU-FSU College of Engineering
Schwartz, J., FAMU-FSU College of Engineering/FSU, Physics/NHMFL

The $Hg_1Ba_2Ca_2Cu_3O_y$ (Hg-1223) superconductor has the highest T_c (135 K) among all the high temperature superconducting cuprates, as well as a significant irreversibility field greater than 0.5 T above 100 K. It has been shown that the stability and superconducting properties of Hg-1223 are greatly improved by partial substitution of Hg by Re, Bi and Pb. It is necessary to develop processing techniques for grain growth and texture, which are essential to make this material suitable for practical applications. We have undertaken a detailed study on doped Hg-1223 materials to evaluate the relative merits of various dopants and their suitability for using them in powder-in-tube or other forms of conductors. Both Bi- and Pb-doping allowed the formation of significant amounts of liquid phase during the reaction and yielded very dense superconducting phase with some degree of texture among the grains (Figure 1). Furthermore, the reaction temperature for (Hg,Bi)- and (Hg,Pb)-1223 are around 850°C, which is suitable for growth of these materials on metals. Role of
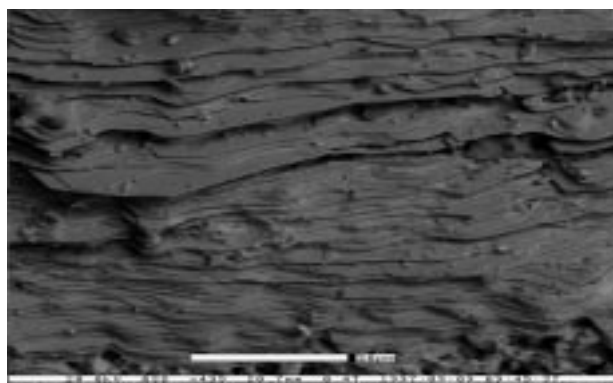
Figure 1. SEM micrograph of a HgBi1223 sample synthesized with $CaHgO_2$ as the external Hg source.

metallic interface on grain alignment of Hg-1223 has been investigated using Ag, Ag-Pd and Au. Samples were characterized for phase purity, microstructure, and interfacial reactions using XRD, SEM and high field (up to 30 T) magnetization measurements (Figure 2). These studies show that the doped Hg-1223 has potential for practical applications at 77 K and higher temperatures.
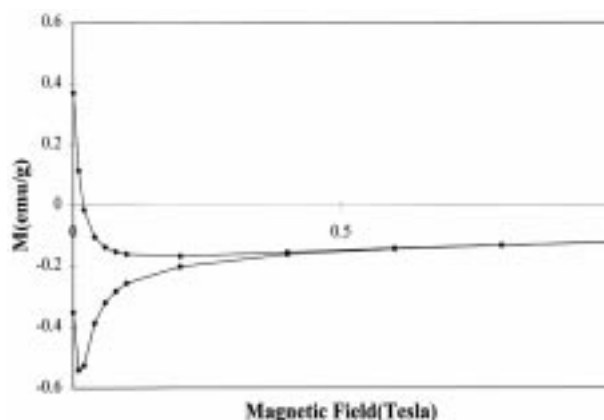
Figure 2. Magnetization vs. field, at 100 K, of a HgPb1223 synthesized with $CaHgO_2$ as the external Hg source.

Effects of Nanosize MgO Addition to $Bi_2Sr_2CaCu_2O_x$

Schwartz, J., NHMFL/FAMU-FSU College of Engineering
Wei, W., NHMFL/FAMU-FSU College of Engineering
Goretta, K.C., Argonne National Laboratory
Balachandra, U., Argonne National Laboratory
Bhargava, A., Univ. of Queensland

Weak flux pinning remains the most serious limitation for the practical applications of $Bi_2Sr_2CaCu_2O_x$ (Bi-2212) at elevated temperatures. This research investigates the possibility of enhancing the flux pinning of Bi-2212 by introducing nanosize MgO particles. The objectives of this research include investigating the phase evolution process, optimizing the heat treatment, and exploring the effects of nanophase doping on the electrical and magnetic behaviors.

The T_c for all the samples as measured by SQUID magnetization is about 85 K, which shows that T_c is virtually unaffected by MgO addition. This is an indication that MgO remain un-reacted after the partial melting process, as the reaction between the oxide addition and the Bi-2212 precursor usually degrades T_c. SEM observations and x-ray analysis also suggests there is no reaction between MgO and the Bi-2212 matrix.

Optimization for the partial melting heat treatment was carried out using different maximum sintering temperatures. Shown in Figure 1 is the relation between transport J_c and maximum heat treatment temperatures for samples with different MgO quantities. Samples with lower MgO additions have comparatively high optimized J_c. J_c value of 70 kA/cm^2 ($I_c = 118$A) was obtained at peak temperature of 910 °C for tape with 11 mol % MgO addition. The optimized maximum heat treatment

Figure 1. Optimization of maximum heat treatment temperature.

Figure 2. Magnetization hysteresis loops obtained by vibrating sample magnetometer measurement up to high magnetic field at 27 K.

temperature is ~10 °C higher than undoped Bi-2212 tapes.

High field vibrating sample magnetometer (VSM) was used to explore the temperature-field range for effective flux pinning in the Bi-2212/MgO samples. Selected results are shown in Figure 2. Nanosize MgO addition expanded the magnetization hysteresis and increased the irreversibility field. This effect increases as the MgO content increases from 11 mol% to 20 mol%.

Further research on critical current density (J_c) at intermediate temperatures and the nano-scale defects associated with the MgO addition is ongoing.

Investigations on BaO$_2$ Additions in Ag-Clad Bi$_2$Sr$_2$CaCu$_2$O$_x$ Wires

Schwartz, J., NHMFL/FAMU-FSU College of Engineering
Trociewitz, U.P., NHMFL/RWTH Aachen Univ. of Technology
Sastry, P.V.P.S.S., NHMFL
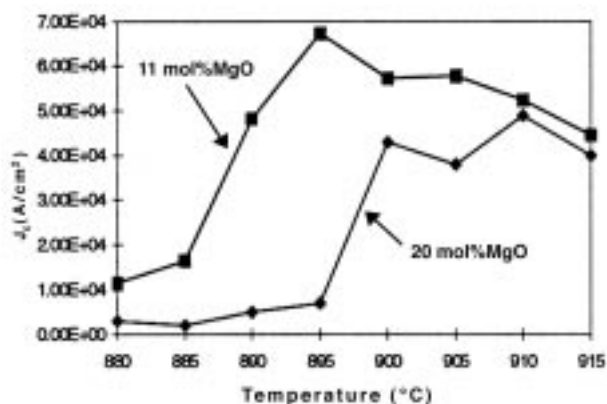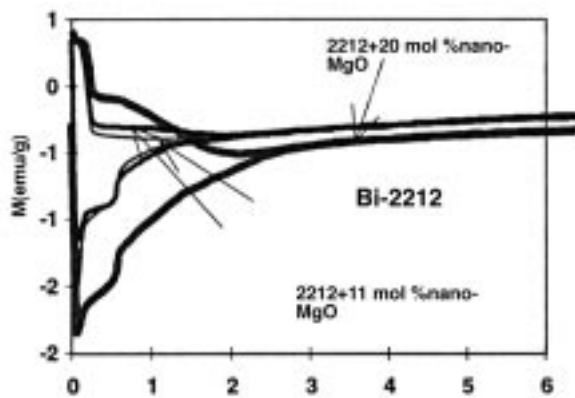Sahm, P.R., RWTH Aachen Univ. of Technology

Among the various materials for high-T_c superconductors, Bi-2212 is one of the most promising for high field applications. The microstructure of partial-melt processed Ag/Bi-2212 tapes exhibit a high degree of texture and uniformity along the Ag-superconductor interface. They are capable of carrying large transport currents at temperatures below 20 K. Applications of Bi-2212 tapes at higher temperatures are limited by weak flux pinning. Here we attempt to improve the flux pinning in Bi-2212 using chemical additions of BaO$_2$. The BaO$_2$ reacts with the Bi-2212 during the heat treatment creating non-superconducting second phases, which serve as pinning centers. Several compositions with varying BaO$_2$ content of bulk samples and Ag-clad wires were studied. Commercially available powder with the stoichiometry Bi$_{2.1}$Sr$_{1.7}$Ca$_{1.2}$Cu$_{2.0}$O$_x$ from SCI and

BaO$_2$ powder from Alfa-Aesar was used in all experiments. Heat treatment processes were varied to optimize the critical current density. Finally the microstructural and electromagnetic properties were investigated. Significant increases in the magnetization and transport properties were obtained. X-ray diffraction data indicate that BaO$_2$ strongly reacts with the precursor. DTA measurements show that the melting temperature is shifted to lower temperatures with increasing amounts of BaO$_2$. Experiments in a SQUID up to 5.5 T and VSM up to 33 T reveal expanded magnetization hysteresis loops in BaO$_2$ added samples. These data indicate a significant influence of reactive additions on flux pinning characteristics of Bi-2212. The SQUID data also show that there is an optimum stoichiometry with 2.38 wt.% BaO$_2$ enhancing the magnetization behavior.
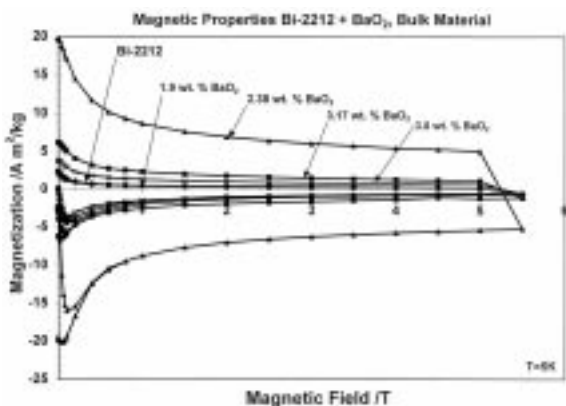
Figure 1. Magnetization hysteresis at 5 K measured with a SQUID in magnetic fields up to 5.5 T for bulk samples with different fractions of BaO$_2$. The curves clearly point an optimum of BaO$_2$ addition for a molar ratio of 8Bi-2212/1BaO$_2$, which equals 2.38 wt.% BaO$_2$.
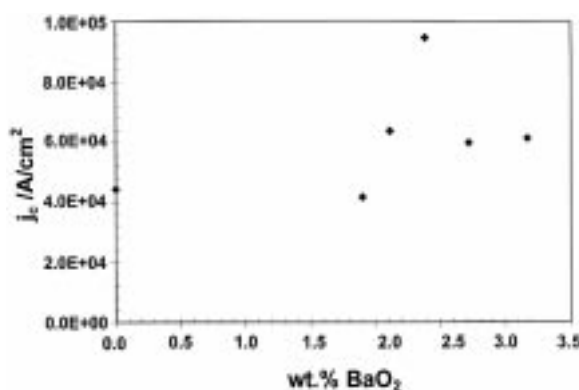
Figure 2. Critical current densities versus BaO$_2$ content. There is an optimum amount of the addition at 2.38 wt.% BaO$_2$.
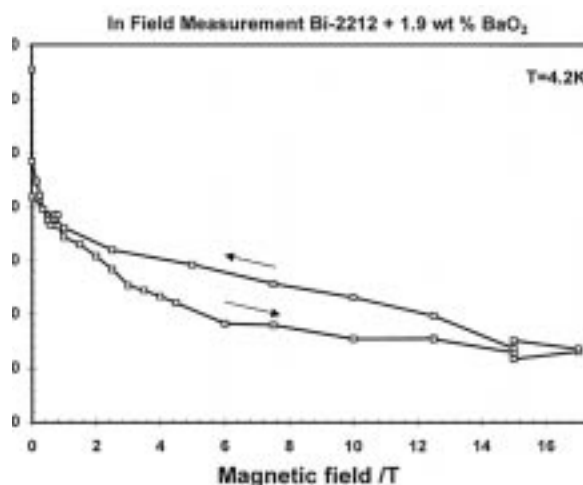
Figure 3. Transport critical current versus magnetic field at 4.2 K for a 1.9 wt.% BaO$_2$ added tape. At a maximum field of 17 T the critical current is 67 A, corresponding to about 50% of the self-field I$_c$. Critical currents for undoped samples typically reach only 30% of the self-field I$_c$ at those fields.

Further additions lead to a decrease in magnetization (Figure 1). Significant improvements of the transport properties of Bi-2212 were demonstrated at 4.2 K in zero field and in field (Figures 2 and 3). At 17 T the critical current drops to about 50% of the zero field value of I$_c$. In earlier studies of undoped Bi-2212, typically only about 30% of the self-I$_c$ remained at 17 T, indicating a positive influence of BaO$_2$ additions. Further studies are necessary to understand the interactions between the reactive additions and the Bi-2212 both in monofilament and multifilament conductors and to further improve the processing conditions.

1 T Class Bi-2212 Insert Coils

Weijers, H.W., NHMFL
Marken, K., Oxford Superconducting Technologies
Hazelton, D., Intermagnetics General Corp.
Hascicek, Y.S., NHMFL
Van Sciver, S., NHMFL/FAMU-FSU College of Engineering
Schwartz, J., NHMFL/FAMU-FSU College of Engineering

As part of the development of a 5 T HTS insert coil that will be part of a 25 T, 1.1 GHz, NMR system,

the NHMFL set an intermediate goal to build an HTS magnet that generates 1 T as an insert magnet in a 50 mm bore and 20 T background field. This 1 T project is carried out in cooperation with industry, specifically Oxford Superconducting Technology and Intermagnetics General Corporation, and focuses on Bi-2212 Wind-and-React (W&R) coils. Additional research was done characterizing React-and-Wind (R&W) conductor and constructing R&W coils. Measurements were performed at the NHMFL, except where stated otherwise.

Wind and React. The double pancake units are wound from one continuous piece of powder-in-tube (PIT) conductor with ZrO_2 insulator. Vacuum epoxy impregnation followed after heat treatment. Successful units were stacked into robust structures.

Coil A consists of 4 units that had I_c's of the remarkably high percentage of 85% of the short sample value. A 17 T background field reduced the coil I_c to 45% of the self field value.

Coil B was stacked as a single unit and tested in the 21 T magnet at the Tsukuba Magnet Lab, NRIM, Japan. The critical current at 21 T was 57 A or 49% of the self field value. No damage occurred despite a hoop stress of about 43 MPa.

Coil C was built using six units, that are more compact then previous units thanks to the use of a new in-house sol-gel insulation application method. The overall packing factor in the winding area is high at 78%. Critical current properties also advanced, leading to a self field of 2.1 T and 1.2 T in a 17 T background, making this a successful 1 T Class coil. The average current density in the windings is 85 A/mm^2, which is considered a useful value for NMR insert magnets and close to the design value for the above mentioned 5 T magnet. A hoop stress induced I_c degradation of 3% at 49 MPa indicates that the conductor was pushed to its limits in the given geometry and that it has become necessary to study re-enforcement in detail. Repeated testing of this coil revealed insensitivity to load cycling or quenches but showed a slight decrease in properties after each thermal cycle, possibly related to the rate of thermal cycling.

React and Wind. R&W development yielded several small pancakes that were used to verify that coil properties at the level of short sample properties are possible and to develop handling procedures for surface coated conductor. Two larger double pancakes were built, tested, and stacked. Their performance was as expected from the short sample characteristics.

R&W and W&R Combined. R&W and W&R techniques both have their advantages and disadvantages. In order to explore the possibilities of magnets that consist of both R&W and W&R sections, to make the best use of the advantages of each approach, this R&W stack was mounted concentrically with Coil C and tested in the 4" bore of our 9 T superconducting magnet. The design of the magnets allowed them to be operated at the same current, to generate a total field of 1.4 T at 63 A in a 9 T background.

Conclusions. We have built a successful 1 T Class coil using PIT double pancake W&R technology. R&W technology shows predictable performance and can be used together with W&R technology.

Stress-Strain and Critical Current Relations in HTS Conductors

Weijers, H.W., NHMFL
Hascicek, Y.S., NHMFL
Amm, B.L., NHMFL
Xiao, L.Y., NHMFL
Van Sciver, S.W., NHMFL/FAMU-FSU College of
    Engineering
Schwartz, J., NHMFL/FAMU-FSU College of
    Engineering

This research explores the relation between the mechanical properties, specifically the stress-strain characteristics, and the critical current of Ag sheeted Bi-2212 superconductors. Both a room-temperature tensile tester and a Lorenz-force based stress-strain device were used in this study.

In-Situ Measurements. In this approach the entire characterization takes place at 4.2 K. Stress is induced by Lorenz force on a circular sample and a capacitive technique allows the determination of strain. Figure 1 shows typical data on a Ag sheeted powder-in-tube (PIT) conductor. The stress is proportional to the strain up to just over 40 MPa stress and 0.25% strain, corresponding to elastic and reversible behavior up to that point. The critical current (I_c), except for some initial settling damage, is unaffected in that range. With the onset of yield, I_c decreases dramatically and irreversibly. The mechanism for degradation is cracking of the ceramic, as evidenced by microstructural analysis. Measurements on surface coated Bi-2212 conductor showed that load cycling has no effect on the critical current.
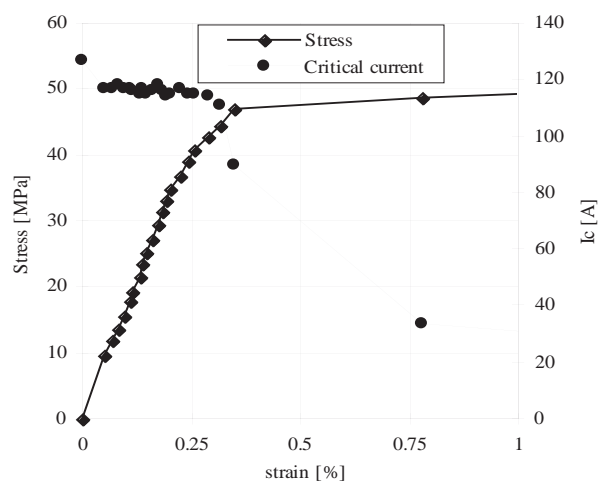
Figure 1. Sample of PIT stress-strain-I_c characteristics at 4.2 K.

Room-Temperature Application of Stress and Strain. A tensile tester was used to measure stress-strain curves at room temperature. Figure 2 shows stress-strain curves of eight samples with unloading after different peak strains. The small decrease in the slope for the unload section of the curves indicates that the ceramic superconductor strengthens the composite structure somewhat until yield occurs, after which the properties of the silver substrate are dominant. After unloading I_c was measured at 4.2 K. These measurements confirm that the onset of yield causes cracks in the superconductor and an abrupt decrease in I_c.
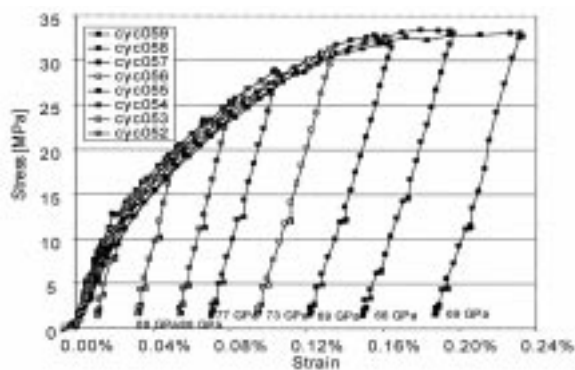
Figure 2. Stress-strain curves of a surface coated conductor at 300 K.

A facility to apply bend strain at room temperature and measure I_c at 77 K was used to characterize candidate Bi-2223 conductors for a transmission cable project of the Southwire Company. These conductors show a very gradual reduction of I_c to about 50% of the straight sample value at 1% strain, making application of those conductors well above the yield strain possible.